PERGAMON

International Journal of Solids and Structures 36 (1999) 2189–2216

INTERNATIONAL JOURNAL OF SOLIDS and STRUCTURES

Geometrical and interfacial non-linearities in the analysis of delamination in composites

Olivier Allix[a]*, Alberto Corigliano[b]†

[a] *Laboratoire de Mécnaique et Technologie, E.N.S. de Cachan/C.N.R.S./Univ. P. et M. Curie. 61, avenue du Président Wilson, 94235 Cachan, France*

[b] *Department of Structural Engineering, Politecnico of Milano piazza Leonardo da Vinci 32, 20133 Milano, Italy*

Received 28 February 1997; in revised form 29 January 1998

Abstract

The subject of this paper is the study of interactions between delamination and geometrical nonlinearities. This problem generally addressed by means of Fracture Mechanics, is here treated by modelling interfacial degradation through irreversible, softening interface constitutive laws. Geometrical nonlinearities are associated to large displacements of thin layers which are assumed to be hyperelastic. A general formulation is presented and then specialised to the case of rectilinear laminated beams. Numerical aspects concerning finite element implementation are discussed together with a local control algorithm for the treatment of unstable paths. Numerical examples showing the effect of interaction between geometrical and material nonlinearities are presented.

1. Introduction

Delamination plays a central role among the degradation phenomena in composite materials. It is generally initiated by large interlaminar stresses due to either edge effects near joints, impacts, concentrated loads or manufacturing defects. The initial delamination can propagate in a stable or unstable way and eventually can be the origin of structural failure.

During the propagation phase, depending on the loading conditions, the delaminated area can reach a critical size and buckling of layers can occur. Buckling can then increase the interlaminar stresses and accelerate the propagation of delamination. Geometrical effects can also be important due to large displacements which show up in thin structures such as those made with composites.

Initiation and propagation of delamination cracks are often studied separately. When a large

* Corresponding author.

† This work has been carried out during a period spent by author A. Corigliano at the Ecole Normale Supérieure de Cachan (France) as visiting professor.

0020–7683/99/$ - see front matter
PII: S0020–7683(98)00079–1

initial delamination defect exists, Fracture Mechanics can be used for the prediction of propagation as is generally done in the existing literature (see e.g. Wang, 1983; Johnson, 1985; Williams, 1988; Pagano 1989). In order to predict initiation (when no initial cracks exist) and propagation specific approaches based on the description of material degradation in the interlaminar region, have to be used. In some works both interlaminar and layer material degradation are modelled (see e.g. Ladevèze, 1992; Allix and Ladevèze, 1994) while more often only interface decohesion is taken into account. This has been done, in the geometrically linear range, through the use of interface constitutive laws which relate tractions to displacement jumps along a surface representing the delamination crack (Allix and Ladevèze, 1992; Daudeville and Ladevèze, 1993; Schellekens and de Borst, 1992; Corigliano, 1993).

Studies which aim at determining critical conditions of propagation when the delaminated area is prone to buckling, generally combine the theory of stability, Fracture Mechanics and numerical simulations. The first works on buckling and growth of delamination are those of Kachanov (1976), Chai et al. (1981), Bottega and Maewal (1983), Evans and Hutchinson (1984). In these works the reference problem concerns the so-called thin film approximation where local buckling of a surface delamination can be dealt with in an analytic form. More recently, approaches based on the evaluation of the Energy Release Rate in a geometrical nonlinear context have been proposed. These allow one to follow, in a finite element context, the propagation of delamination induced by buckling (see e.g. Storakers and Andersson, 1988; Storakers and Nilsson, 1993). In order to compute the nonlinear response preceding delamination, asymptotic-numeric methods based on perturbation analysis have been used to obtain low-cost information about the critical load and the initial post-buckling behaviour with small range propagation of the delaminated area (see e.g. Cochelin and Potier-Ferry, 1991; Cochelin et al. 1993; Kardomateas, 1993). Buckling induced delamination has also been treated through the use of elastic springs with finite strength for the simulation of decohesion in Bruno and Grimaldi (1990).

The purpose of the present paper is the study of delamination processes by means of a unified formulation which takes into account initiation and propagation together with geometrical effects. This is accomplished by making use of interface models for the description of material degradation along the layer connections and of a large displacement formulation.

In order to make use of interface models developed in the linear geometry range, it is here introduced the fundamental hypothesis that displacement discontinuities (jumps) along delamination surfaces are small before the local complete failure of interlaminar connection. Due to this hypothesis, it is possible to define an interface (delamination surface) which follows the current configuration of the body (laminated) and over which material degradation modelled by an interface constitutive law takes place. After complete separation along the interface, the contact conditions of the separated surfaces are treated in an approximate way, thus allowing the use of special interface laws also for the description of contact conditions.

The proposed formulation allow the complete study of delamination processes, from initiation to structural failure. In particular delamination–buckling interaction can be studied and propagation of post buckling delamination can be followed.

The present work is a generalisation to the case of nonlinear geometric effects of previous works, Allix, et al. (1994) and Allix and Corigliano (1996), where fracture propagation in delamination specimens in pure and mixed mode conditions has been studied.

An outline of the paper is as follows. In Section 2 the basic assumptions of the proposed

formulation are discussed and the governing equations are introduced, an elastic–damage interface law is described. The formulation proposed in Section 2 is particularised in Section 3 to the case of laminated rectilinear beams. Some details on the finite element implementation and on the solution strategy are discussed in Section 4. In Section 5 simple numerical examples are presented and discussed concerning mode I delamination.

2. Basic hypotheses and formulation

Consider a body Ω in which a set of m surface Γ_i is embedded. The surfaces Γ_i, called henceforth interfaces, are loci of possible displacement discontinuities due to decohesion processes such as delamination in composite materials, which cause a progressive decreasing of cohesive stresses, until possible complete separation. The set of all interfaces is referred to as Γ, while Ω' denotes $\Omega - \Gamma$.

The problem under discussion is the study of the response of the body Ω, subject to a given loading process which is a cause of large displacements from the starting configuration, while the interface Γ can be progressively damaged until complete separation of the two parts of the body Ω initially in contact along Γ. In Fig. 1 a schematic representation of the solid Ω containing an interface Γ is shown. The interface Γ separates Ω in two parts denoted with $+$ and $-$, the normal $\mathbf{n}$ to Γ is directed toward the positive part of Ω.

The study of the above problem is based on the following assumptions and hypotheses:

(a) large displacements are possible in the body Ω';

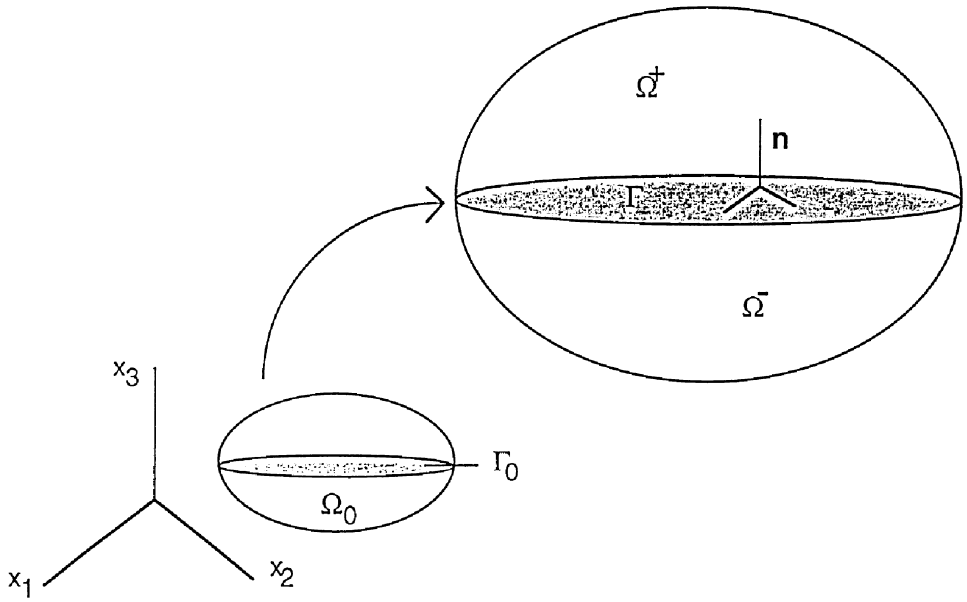

Fig. 1. Schematic representation of two solids Ω in contact through an interface Γ.

(b) the behaviour of the body Ω' is hyperelastic;
(c) along Γ the displacements can be large but the displacement discontinuities are small in the non-fully delaminated part of the specimen or in the contact region;
(d) an irreversible, softening behaviour is attributed to Γ by means of an interface law connecting tractions to displacement discontinuities;
(e) isothermal conditions are assumed;
(f) the loads do not depend on the configuration of the body, i.e. follower forces are not considered.

Hypotheses (a) and (b) characterise the behaviour of the body Ω' as a whole. These can be applied to the study of many real cases, in particular they allow the study of the influence of geometrical effects on delamination in composite materials and therefore of buckling-induced delamination. Hypothesis (c) specifies the constitutive behaviour of the interlaminar connection and situations where the parts of the interfaces which come into contact are close to the delamination front. This simplification corresponds to situations often encountered for crack propagation in laminates, adhesives, glues and rubber connection....

Let us define by Ω'_0 and Γ_0 the configurations of the body and of the interfaces at time $\tau = 0$. These are considered as reference configurations during the transformation process.

The displacement discontinuity vector $[\mathbf{u}]$ on the interface is given by the difference of displacements pertaining to positive and negative parts (see Fig. 1):

$$[\mathbf{u}] = (m_+ - m_-)(m_0) \quad m_0 \in \Gamma_0 \tag{1}$$

where points in the reference and current configurations have been noted by m_0 and m, respectively.

Each interface Γ_0 is initially divided in a completely cracked part $\Gamma_{0d}(\tau = 0)$ (e.g. an initial delamination in composites) and a part $\Gamma_{0nd}(\tau = 0)$ on which the cohesion between Ω^+ and Ω^- is complete. The initial delaminated region is composed of points which are in contact but through which no cohesive tractions can be transmitted. During the loading process the delaminated part $\Gamma_{0d}(\tau)$ (seen as the image of the reference configuration) can increase; moreover in the delaminated region it is possible to have points of parts Ω^+ and Ω^- which loose contact, regain contact after separation, or remain in contact. In the present work no true contact conditions are considered between the two surfaces of the delaminated part, the contact points which are taken into account are only those which were in the same position in the initial configuration, they are the image of the set called $\Gamma_{0c}(\tau)$. The point which are separated are the image of the set called $\Gamma_{0s}(\tau)$.

Due to the above considerations the reference interface Γ_0 at a time instant τ is partitioned as: $\Gamma_0 \equiv \Gamma_{0nd}(\tau) \vee \Gamma_{0c}(\tau) \bigcup \Gamma_{0s}(\tau)$.

The definition of the current image of $\Gamma_{0nd}(\tau)$ is based on hypothesis (c). With this hypothesis a separation of the body Ω' in two parts is allowed, along the non-delaminated region of the interface, but this must be small with respect to a characteristic length of the surface Γ_0. It is therefore possible to define a unique interface $\Gamma_{nd}(\tau)$ in the deformed configuration, to which an interface law can be attributed following hypothesis (d). The definition of $\Gamma_{nd}(\tau)$ is based on the mean value $\mathbf{u}_m(m_0)$ of displacements relevant to positive and negative sides (see Figs 1 and 2).

$$\mathbf{u}_m(m_0) \equiv \frac{m^+ + m^-}{2}; \quad \Gamma_{nd}(\tau) \equiv \{m/m \in \Gamma_{0nd}(\tau; \quad m = m_0 + \mathbf{u}(m_0)\} \tag{2}$$

With the above definition $\Gamma_{nd}(\tau)$ is seen as a mean surface between the upper and lower displaced

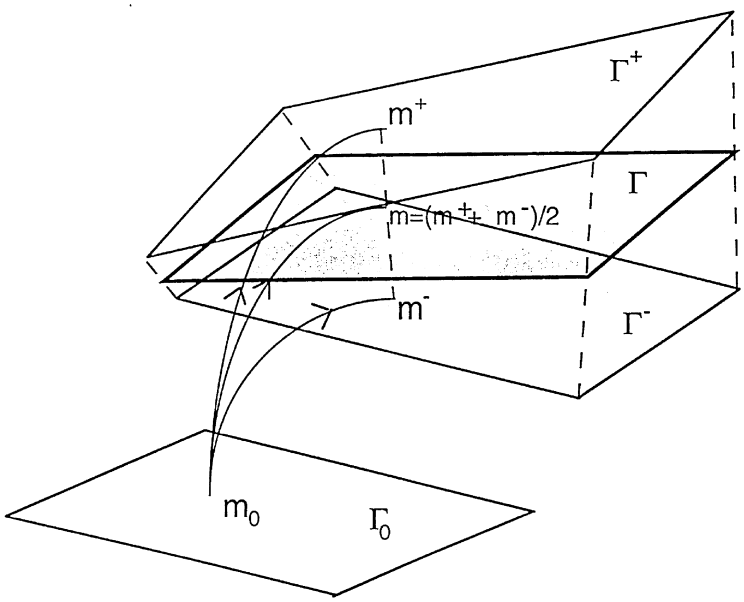

Fig. 2. Graphical definition of the interface Γ.

parts, which in fact can be considered to be geometrically coincident thanks to hypothesis (c). $\Gamma_{nd}(\tau)$ can thus be viewed as a zero-thickness medium which ensures stress transfer from one part to another. Hence it is possible to define an interface law as a relation between the interface traction vector $\mathbf{t}$ and the displacement discontinuity vector $[\mathbf{u}]$. The interface traction vector $\mathbf{t} = \boldsymbol{\sigma}\mathbf{n}$ is the component of the Cauchy stress tensor $\boldsymbol{\sigma}$ along the direction $\mathbf{n}$ normal to the interface, in the current configuration.

Account taken of what precedes, the definition of $\Gamma_c(\tau)$ is the following:

$$\Gamma_c(\tau) \equiv \{m/m_0 \in \Gamma_{0c}(\tau)\,; \quad m = m_0 + \mathbf{u}_m(m_0\,; \quad [\mathbf{u}](m_0) \cdot \mathbf{n} = 0\} \tag{3}$$

On the part $\Gamma_c(\tau)$ unilateral contact conditions, with or without friction, can be imposed by means of an interface law, as shown in Section 2.2, thus implying the same kind of treatment for parts $\Gamma_{nd}(\tau)$ and $\Gamma_c(\tau)$.

A definition of $\Gamma_s(\tau)$ is not necessary for the solution of the problem under discussion, due to the fact that tractions are not transmitted along the delaminated and not in contact parts, and to the approximate definition given for the set of contact points.

2.1. Equilibrium and elastic behaviour of the body

For the sake of simplicity let us denote in what follows with the symbol Γ the sum of parts $\Gamma_{nd}(\tau)$ and $\Gamma_c(\tau)$ of the current interface.

Equilibrium of the body Ω in the current configuration can be expressed through the virtual power principle:

$$\int_{\Omega'} \boldsymbol{\sigma} : \mathbf{D}^*(\mathbf{v}^*)\,\mathrm{d}\Omega + \int_{\Gamma} \mathbf{t}\cdot[\mathbf{v}]^*\,\mathrm{d}\Gamma = \mathbf{P}_e^* \quad \text{for any } \mathbf{V}^* \in \mathscr{V}; \quad \mathbf{D}^* = \frac{1}{2}\left(\frac{\partial \mathbf{v}^*}{\partial m} + \left(\frac{\partial \mathbf{v}^*}{\partial m}\right)^{\mathrm{T}}\right) \tag{4}$$

In the above equation: $\mathscr{V}$ is the set of kinematically admissible velocity vectors $\mathbf{v}^*$; $\boldsymbol{\sigma}$ is the Cauchy stress tensor; $\mathbf{D}^*$ is the rate of deformation tensor; $[\mathbf{v}]^* = \mathbf{v}^*(m_+) - \mathbf{v}^*(m_-)$ is the velocity discontinuity vector defined on Γ; $\mathbf{P}_e^*$ is the power of external loads.

Hypothesis (b) allows one to conveniently use Lagrangian tensors for the expression of the internal power relevant to be the hyperelastic body Ω'. The first term in eqn (4) can then be rewritten as:

$$\int_{\Omega'} \boldsymbol{\sigma} : \mathbf{D}^*\,\mathrm{d}\Omega = \int_{\Omega_0} \Pi : \dot{\mathbf{E}}^*\,\mathrm{d}\Omega_0 \tag{5}$$

where Π denotes the second Piola–Kirchhoff stress tensor and $\dot{\mathbf{E}}$ the rate of the Lagrangian strain tensor. $\dot{\mathbf{E}}$ is related to the Cauchy stress $\boldsymbol{\sigma}$, to the rate of deformation $\mathbf{D}$ and to the deformation gradient $\mathbf{F}$ by the following relations:

$$\Pi = J\mathbf{F}^{-1}\boldsymbol{\sigma}(\mathbf{F}^{-1})^{\mathrm{T}}; \quad \dot{\mathbf{E}} = \mathbf{F}^{\mathrm{T}}\mathbf{D}\mathbf{F}; \quad \mathbf{F} = \frac{\partial m}{\partial m_0}; \quad J = \det \mathbf{F} \tag{6}$$

It is also useful to recall the expression of the Lagrangian strain $\mathbf{E}$ tensor as a function of the displacement field $\mathbf{u}$:

$$\mathbf{E} = \frac{1}{2}\left(\left(\frac{\partial \mathbf{u}}{\partial m_0}\right)^{\mathrm{T}} + \frac{\partial \mathbf{u}}{\partial m_0} + \left(\frac{\partial \mathbf{u}}{\partial m_0}\right)^{\mathrm{T}}\frac{\partial \mathbf{u}}{\partial m_0}\right) \tag{7}$$

The hyperelastic constitutive law in the body Ω' is here expressed through the introduction of a convex functional $\Psi(\mathbf{E})$ such that:

$$\Pi = \frac{\partial \Psi(\mathbf{E})}{\partial \mathbf{E}} \tag{8}$$

After the introduction of eqns (5) and (8) in the virtual power principle (3), this can be rewritten in the following form:

$$\int_{\Omega_0'} \frac{\partial \Psi(\mathbf{E})}{\partial \mathbf{E}} : \dot{\mathbf{E}}^*\,\mathrm{d}\Omega_0 + \int_{\Gamma} \sigma\mathbf{n}\cdot[\mathbf{v}]^*\,\mathrm{d}\Gamma = \mathbf{P}_e^*;$$

$$\text{for any } \mathbf{v}^* \in \mathscr{V}, \quad \dot{\mathbf{E}}^* = \mathbf{F}^{\mathrm{T}}\mathbf{D}^*\mathbf{F}, \quad \mathbf{D}^* = \frac{1}{2}\left(\frac{\partial \mathbf{v}}{\partial m} + \left(\frac{\partial \mathbf{v}^*}{\partial m}\right)^{\mathrm{T}}\right) \tag{9}$$

2.2. Interface constitutive law

Hypothesis (c) introduced at the beginning of Section 2 has allowed the definition of an interface Γ in the current configuration. It is therefore now possible to speak about interface points and interface quantities. As already observed in the introduction of the paper, the interface is introduced

in order to be able to simulate decohesion processes which can occur in layered composites or, more generally, in elastic media with concentrated damage.

The simulation of decohesion can be obtained through the formulation of irreversible, softening interface laws, as assumed in hypothesis (d). In the interface constitutive law displacement discontinuities play the role of deformations, while traction vectors on the surface Γ play the role of stresses. The assumption that displacement discontinuities are small allows the use of interface laws formulated in the small perturbation case, provided that the interface quantities are evaluated in the current configuration with reference to a frame conveniently connected with the current interface Γ.

It is useful to notice that interface quantities $\mathbf{t}$, $[\mathbf{u}]$ and $[\mathbf{v}]$ are frame indifferent if hypothesis (c) is satisfied, i.e. they transform respecting the transformation rules of vectors. Consider in fact the transformed coordinates of two points associated to the positive and negative parts of the interface.

$$\mathbf{x}_+^* = \mathbf{c} + \mathbf{Q}\mathbf{x}_+, \quad \mathbf{x}_-^* = \mathbf{c} + \mathbf{Q}\mathbf{x}_-, \tag{10}$$

where $\mathbf{c}$ and $\mathbf{Q}$ are the position vector and the rotation matrix of the new reference frame with respect to the old one. The rule of transformation of the displacement discontinuity vector can be derived from eqns (10) by simply taking the difference of the two expressions: $[\mathbf{u}]^* = \mathbf{Q}[\mathbf{u}]$. From the difference of the time derivatives of eqns (10) the transformation rule for the velocity discontinuity vector can be obtained:

$$[\mathbf{v}]^* = \dot{\mathbf{Q}}[\mathbf{x}_+ - \mathbf{x}_-] + \mathbf{Q}[\mathbf{v}] \tag{11}$$

From the above equation it can be concluded that the vector $[\mathbf{v}]$ is frame indifferent if hypothesis (c) is satisfied, i.e. if $[\mathbf{x}_+ - \mathbf{x}_-] \cong \mathbf{0}$.

In this section two examples of interface laws are presented. The first one is elastic while the second one is elastic–damage. The elastic–damage law is an example of interface laws satisfying hypothesis (d).

2.3. Elastic interface law

An anisotropic elastic interface law can be formulated as a relation between the traction vector $\mathbf{t}$ and the displacement discontinuity vector $[\mathbf{u}]$ in which a dependence on the current orientation of the interface Γ is introduced by means of the normal $\mathbf{n}$ to Γ.

$$\mathbf{t} = g([\mathbf{u}], \mathbf{n}) \tag{12}$$

In this case the respect of the principle of material frame indifference implies the satisfaction of the following relation:

$$\mathbf{Q}g([\mathbf{u}], \mathbf{n}) = g(\mathbf{Q}[\mathbf{u}], \mathbf{Q}\mathbf{n}) \tag{13}$$

An example of linear case of the law (12) can be formulated as follows:

$$t_\mathrm{n} = K_\mathrm{n}[u]_\mathrm{n}, \quad \mathbf{t}_\mathrm{t} = K_\mathrm{t}\mathbf{P}[\mathbf{u}] = K_\mathrm{t}[\mathbf{u}]_\mathrm{t} \tag{14}$$

where the normal components t_n, $[u]_\mathrm{n}$ and the tangent projections $\mathbf{t}_\mathrm{t}$, $[\mathbf{u}]_\mathrm{t}$ of the traction and displacement discontinuity vectors have been distinguished. K_n and K_t are interface elastic stiff-

nesses, with the dimension of a force over length cube; $\mathbf{P}=(\mathbf{I}-\mathbf{nn}^{\mathrm{T}})$ is the projection operator on the surface Γ. It can be shown that relations (14) satisfy eqn (13).

2.4. Elastic-damage interface law

An example of elastic–damage interface law is here presented having in mind as main application the study of delamination, i.e. the debonding of adjacent layers in composite materials. In this case the level of tractions $\mathbf{t}$ which can be transmitted between the layers, decreases with the opening or sliding of adjacent layers until a critical level $[\mathbf{u}]_{\mathrm{c}}$ is reached. The layers are then completely separated.

A strain energy for unit surface of the damageable interface is first defined as follows:

$$E_{\mathrm{d}}=\tfrac{1}{2}(1-d_{\mathrm{n}})K_{\mathrm{n}}^{+}\langle[u]_{\mathrm{n}}\rangle_{+}^{2}+\tfrac{1}{2}K_{\mathrm{n}}^{-}\langle[u]_{\mathrm{n}}\rangle_{-}^{2}+\tfrac{1}{2}(1-d_{\mathrm{t}})K_{\mathrm{t}}\parallel[\mathbf{u}]_{\mathrm{t}}\parallel^{2} \tag{15}$$

where d_{n}, d_{t} are two non-dimensional scalar damage variables which vary between 0 (no damage) and 1 (total damage); K_{n}^{+}, K_{n}^{-}, K_{t} are interface stiffnesses as in eqns (14). The symbols $\langle\cdot\rangle_{+}$ and $\langle\cdot\rangle_{-}$ denote the positive and negative parts of $\cdot$; these are introduced in the strain energy in order to take into account the unilateral effect, i.e. the difference in tensile and compressive behaviour for the direction $\mathbf{n}$ normal to the surface; as a consequence different values K_{n}^{+} and K_{n}^{-} of interface stiffnesses for tension and compression have also been introduced. $\|[\mathbf{u}_{\mathrm{t}}]\|$ denotes the Euclidean norm of the tangent projection of $[\mathbf{u}]$ on Γ.

The tractions t_{n}, $\mathbf{t}_{\mathrm{t}}$ and the damage energy release rates Y_{n}, Y_{t} (energies per unit surface) associated to damage variables are obtained by computing derivatives of the strain energy:

$$t_{\mathrm{n}}=\frac{\partial E_{\mathrm{d}}}{\partial[u]_{\mathrm{n}}}=(1-d_{\mathrm{n}})K_{\mathrm{n}}^{+}\langle[u]_{\mathrm{n}}\rangle_{+}+K_{\mathrm{n}}^{-}\langle[u]_{\mathrm{n}}\rangle_{-};\quad \mathbf{t}_{\mathrm{t}}=\frac{\partial E_{\mathrm{d}}}{\partial[\mathbf{u}]_{\mathrm{t}}}=(1-d_{\mathrm{t}})K_{\mathrm{t}}[\mathbf{u}]_{\mathrm{t}} \tag{16}$$

$$Y_{\mathrm{n}}=-\frac{\partial E_{\mathrm{d}}}{\partial d_{\mathrm{n}}}=\frac{1}{2}K_{\mathrm{n}}^{+}\langle[u]_{\mathrm{n}}\rangle_{+}^{2};\quad Y_{\mathrm{t}}=-\frac{\partial E_{\mathrm{d}}}{\partial d_{\mathrm{t}}}=\frac{1}{2}K_{\mathrm{t}}\parallel[\mathbf{u}]_{t}\parallel^{2} \tag{17}$$

The evolution of damage phenomena is governed through a non-dimensional damage function f_{d}, loading–unloading conditions and non-associated evolution laws for damage variables d_{n}, d_{t}

$$f_{\mathrm{d}}=f(Y_{\mathrm{n}},Y_{\mathrm{t}})-\bar{Y}-1 \tag{18}$$

$$f_{\mathrm{d}}\leqslant 0;\quad f_{\mathrm{d}}\dot{\lambda}=0;\quad \dot{\lambda}\geqslant 0 \tag{19}$$

$$\dot{\bar{Y}}=\dot{\lambda};\quad \dot{d}_{\mathrm{n}}=l_{\mathrm{n}}(\bar{Y})\dot{\lambda};\quad \dot{d}_{\mathrm{t}}=l_{\mathrm{t}}(\bar{Y})\dot{\lambda} \tag{20}$$

The function f is positive, convex and differentiable, $f(0)=0$. It is worth noting that the evolution law for damage variables can be equivalently expressed as follows:

$$\bar{Y}=\sup\left\{1,\sup_{\tau'\leqslant\tau}\{f(Y_{\mathrm{n}},Y_{\mathrm{t}})\}\right\}-1 \tag{21}$$

$$d_{\mathrm{n}}=L_{\mathrm{n}}(\bar{Y})\equiv\int_{0}^{\bar{Y}}l_{\mathrm{n}}(\bar{Y}')\,\mathrm{d}\bar{Y}';\quad d_{\mathrm{t}}=L_{\mathrm{t}}(\bar{Y})\equiv\int_{0}^{\bar{Y}}l_{\mathrm{t}}(\bar{Y}')\,\mathrm{d}\bar{Y}' \tag{22}$$

where τ is the current time instant. The following restrictions precise the chosen damage evolution law.

$$L(0) = 0; \quad 0 \leqslant L(\bar{Y}) \leqslant 1; \quad \frac{\mathrm{d}L(\bar{Y})}{\mathrm{d}\bar{Y}} \geqslant 0 \tag{23}$$

$$d_{\mathrm{n}} = 1 \Rightarrow d_{\mathrm{t}} = 1 \tag{24}$$

In view of the above eqns (22) the evolution of the damage variables is governed by the choice of functions $L_{\mathrm{n,t}}(\bar{Y})$ subject to conditions (23). Relation (24) implies that when complete damage is reached for mode I (opening mode, in direction n, cf. Fig. 1), the interface is considered completely damaged in modes II and III (shearing modes, on the tangent plane) too.

The above elastic–damage interface law can be interpreted as a modification, due to the presence of damage variables, of the elastic law presented previously. In addition to the elastic case, it must therefore be verified the frame indifference of the damage evolution law. This is assured by the fact that the damage law is expressed using frame indifferent scalar functions of time, i.e. Y_{n}, Y_{t}. It can be noticed that no objective rates have been explicitly used for the formulation of the interface constitutive law. This is due to the fact that the evolution of damage depends only on the component of the vectors along the normal **n** to the interface and on the norm of the projection on the tangent plane.

The model presented is isotropic on the tangent plane, it takes partially into account the anisotropy of the response connected to the behaviour of composite materials. The two damage variables evolve at the same time, but the velocity of evolution can be independently governed by the choice of functions $L_{\mathrm{n,t}}(\bar{Y})$. The quantity chosen to govern the damage criterion is a norm of energy variables associated to damage. A particular choice which will be used for the numerical examples of Section 5 is the following:

$$f_{\mathrm{d}} = \sqrt{(a_{\mathrm{n}} Y_{\mathrm{n}})^{\alpha} + (a_{\mathrm{t}} Y_{\mathrm{t}})^{\alpha}} - \bar{Y} - 1; \quad L_{\mathrm{n}}(\bar{Y}) = \gamma_{\mathrm{n}} \bar{Y}; \quad L_{\mathrm{t}}(\bar{Y}) = \lambda_{\mathrm{t}} \bar{Y} \tag{25}$$

where a_{n}, a_{t} are nonnegative model parameters with the dimension of the inverse of Y_{n}, Y_{t}; α, γ_{n}, γ_{t} are non-dimensional positive parameters.

The presented elastic–damage model depends on eight parameters: the elastic stiffnesses K_{n}^{+}, K_{n}^{-}, K_{t}; the damage function parameters a_{n}, a_{t}, α and the damage evolution parameters γ_{n}, γ_{t}. The values of interface stiffnesses can be computed as: $K_{\mathrm{t}} \cong 2G_{\mathrm{tn}}/e$; $K_{\mathrm{n}}^{+} \cong E_{\mathrm{nn}}/e$ where G_{tn}, and E_{nn} are shear and Young moduli of an ideal layer of thickness e representing the interface. For numerical applications G_{tn}, and E_{nn} can be assumed equal to the analogous values of an homogenised layer of the composite or to the values attributed to the matrix; e can be assumed equal to a fraction of the layer thickness. Parameter K_{n}^{-} is the interface stiffness for compression in direction normal to the interface; it is introduced in order to model the unilateral effect and it can be considered as a penalisation parameter that allow one to satisfy unilateral constraint conditions; for this reason it must be chosen with a high value, for simplicity it can also be made equal to K_{n}^{+}. Parameters a_{n}, a_{t} are connected to damage initiation. They can be identified with the inverse of damage initiation energies in pure mode I and in shear mode situations, i.e.: $a_{\mathrm{n}} = 1/Y_{0\mathrm{n}}$, $a_{\mathrm{t}} = 1/T_{0\mathrm{t}}$. α can be identified starting from information connected to the behaviour in mixed mode situations. Parameters γ_{n}, γ_{t} can be evaluated from the knowledge of fracture energies in pure mode I and in shear modes, respectively.

A deeper discussion on the identification of a damage model similar to that here presented can be found in Allix and Corigliano (1996). A recent experimental study on delamination specimens can be found in Allix et al. (1996) where particular attention has been paid on the dependence of interface properties on the fibre direction.

2.5. Remarks

(i) Damage interface laws can be interpreted as a generalisation of the model of elastic springs with softening. They allow the simulation of pure and mixed-mode situations. Through the use of interface laws, inelastic effects, possibly associated with friction, can be easily taken into account by introducing a decomposition of the displacement jump in an elastic and an inelastic part; viscous effects can be taken into account as well.

(ii) Based on its definition, the interface Γ is seen as a medium subject to large transformations but small deformations, the deformation measure being represented by the displacement discontinuity vector $[\mathbf{u}]$.

(iii) The proposed formulation allows the study of delamination phenomena in layered composites, particularly coupled with buckling of the laminae. Other practical applications can be considered such as the initiation and propagation of defects and fracture in rubber-like materials and the study of adhesive layers.

(iv) As seen in Section 2.2, unilateral contact conditions can be introduced in the formulation by means of unilateral effects in the interface law. The same kind of unilateral conditions can be applied to the part $\Gamma_c(\theta)$ of the current interface, thus avoiding inter-penetration. As already observed at the beginning of the present Section 2, the study of a true contact problem has been ruled out from the present formulation.

(v) In previous works use has been made of orthotropic interface laws in the linear geometric case. Orthotropic directions were chosen as the normal to the interface and the bisectors of the fibres of adjacent layers. This choice could be extended to the non-linear range.

(vi) Interface laws can be expressed in a complete rate form. In that case the objective rate used must be associated to the rotation of the normal $\mathbf{n}$ to the interface. To complete the definition of the rotation one can, for example, introduce two orthogonal directions of the tangent plane of Γ which remains orthogonal in the infinitesimal displacement. They are associated to unit eigenvectors of the operator $\mathbf{P}\cdot(\partial\mathbf{v}_m/\partial m)_{sym}\cdot\mathbf{P}$

3. Application to two-dimensional laminated rectilinear beams

In this Section the general formulation presented in the previous Section 2 is particularised to the case of laminated rectilinear beams studied in two dimensions. This particularisation allows one to exemplify what is described in Section 2 in general terms and is particularly useful for the study of delamination specimens subject to cylindrical bending states, as shown in Section 5.

Consider a laminated beam composed by n layers such that drawn in Fig. 3. The reference frame is not associated to a particular layer; the thickness of layer i is given by $h_i = (x_3^{i+1} - x_3^i)$. The elastic body Ω' *defined in Section* 2 *coincides in the present case with the set of* n layers. The set of interfaces

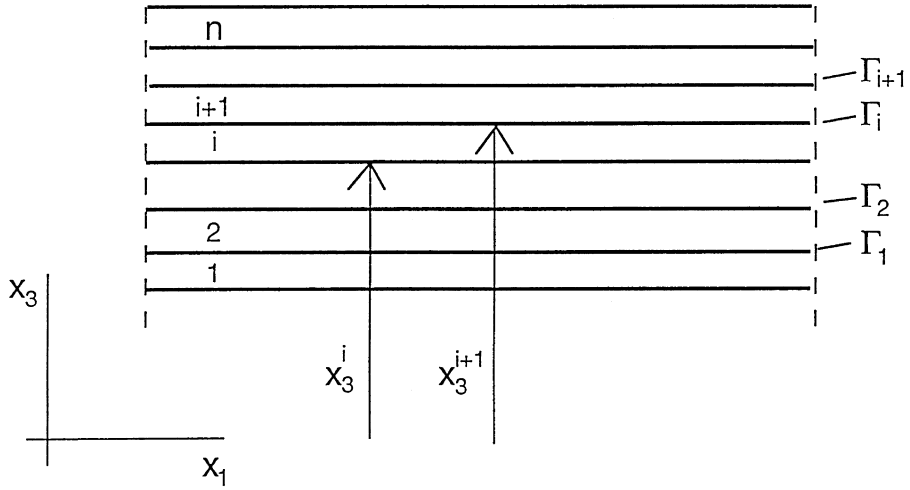

Fig. 3. Deformable beams in contact through an interface Γ.

Γ is represented by the $(n-1)$ line of connections between adjacent layers, damaging interfaces simulate progressive delamination of the beam.

A kinematic hypothesis for each of the layers composing the laminated is first introduced in Section 3.1 and its consequences on the description of the problem in terms of generalised variables are deduced. In Section 3.2 it is shown how the interface quantities can be practically evaluated.

3.1. Description of the layers

Each layer of the laminated is supposed to behave like a beam, obeying the Timoshenko kinematic. Moreover Π_{33} is assumed to be negligible due to the small thickness over length ratio. The displacement field for each point in the i-th layer, having the initial position (x_1, x_3), is defined as (see Fig. 4):

$$u_1^i(x_1, x_3) = u_0^i(x_1) + x_3\theta^i(x_1); \quad u_2^i = 0; \quad u_3^i = w_0^i(x_1) \tag{26}$$

In the above equations, u_1^i, u_2^i, u_3^i are displacement components in directions x_1, x_2, x_3, respectively; u_0^i and w_0^i are the components of the displacement vector of a reference point $m_0(x_1)$ which is found at the intersection of the x_1 axis with the prolongation of the beam section (see Fig. 4); θ^i is the rotation of the beam section with respect to the fixed direction x_3. Functions u_0^i, w_0^i and θ^i are generalised displacements for the layer, collected in vector **s**.

The above kinematic hypotheses introduced for the layer are motivated by the importance of shear deformation in composite specimens. They are similar to those used, among others, by Kanninen (1973) and Whitney (1989) for the analysis of DCB and ENF specimens and represent a particularisation to the two-dimensional case of the Reissner–Mindlin kinematic for plates.

Following the above hypotheses the contribution of a single layer i to the internal power of the elastic body Ω' [eqn (9)] can be expressed as:

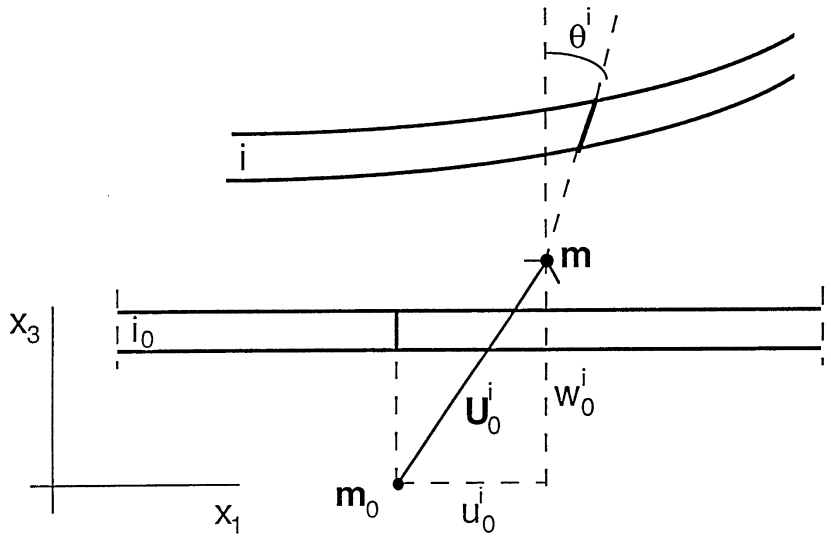

Fig. 4. Kinematic hypothesis for the layers.

$$\left(\int_{\Omega_0'} \frac{\partial \Psi(\mathbf{E})}{\partial \mathbf{E}} : \dot{\mathbf{E}}\, \mathrm{d}\Omega_0\right)_i = \int_{x_1}\int_{A_i} (\Pi_{11}\dot{E}^*_{11} + 2\Pi_{13}\dot{E}^*_{13})_i\, \mathrm{d}A\, \mathrm{d}x_1 \tag{27}$$

In the above equation the integral over the layer volume has been split in an integral over the length and an integral over the section area A.

E^*_{11} and E^*_{13} can be computed after the introduction of the displacement field (26) in the expression of the Green–Lagrange strain tensor (7). One thus obtains:

$$E_{11} = \frac{\mathrm{d}u_0}{\mathrm{d}x_1} + x_3\frac{\mathrm{d}\theta}{\mathrm{d}x_1} - \frac{1}{2}\left(\frac{\mathrm{d}w_0}{\mathrm{d}x_1}\right)^2 + \left[\frac{1}{2}\left(\frac{\mathrm{d}u_0}{\mathrm{d}x_1} + x_3\frac{\mathrm{d}\theta}{\mathrm{d}x_1}\right)^2\right] \tag{28a}$$

$$E_{13} = \frac{1}{2}\left(\frac{\mathrm{d}w_0}{\mathrm{d}x_1} - \frac{\mathrm{d}w_0}{\mathrm{d}x_1}\right) + \left[\frac{\theta}{2}\left(\frac{\mathrm{d}u_0}{\mathrm{d}x_1} + x_3\frac{\mathrm{d}\theta}{\mathrm{d}x_1}\right)\right] \tag{28b}$$

where the superscript i has been omitted for brevity as in the following of this sub-section.

The above relations (28) are here used neglecting the terms in square brackets, thus obtaining a formulation which differ from the linear geometry case for the presence of the term $\frac{1}{2}(\mathrm{d}w_0/\mathrm{d}x_1)^2$ in the expression of E_{11} only. This assumption is equivalent to the moderate rotation hypothesis of the von Karman plate theory which was used, among others, by Storakers and Andersson (1988), Cochelin and Potier–Ferry (1991) for the study of buckling-induced delamination.

By computing time derivatives of E_{11}, E_{13} in eqn (28), the internal power relevant to a single layer [eqn (27)] can be rewritten as:

$$\int_{x_1}\left[\left(\int_A \Pi_{11}\,\mathrm{d}A\right)\left(\frac{\mathrm{d}\dot{u}_0}{\mathrm{d}x_1}+\frac{\mathrm{d}w_0}{\mathrm{d}x_1}\frac{\mathrm{d}\dot{w}_0}{\mathrm{d}x_1}\right)+\left(\int_A \Pi_{11}x_3\,\mathrm{d}A\right)\left(\frac{\mathrm{d}\dot{\theta}}{\mathrm{d}x_1}\right)+\left(\int_A \Pi_{13}\,\mathrm{d}A\right)\left(\dot{\theta}+\frac{\mathrm{d}\dot{w}_0}{\mathrm{d}x_1}\right)\right]_i \mathrm{d}x_1 \equiv \int_{x_1}\mathbf{Q}^{\mathrm{T}}\dot{\mathbf{q}}\,\mathrm{d}x_1 \quad (29)$$

In the above equation, vectors of static $\mathbf{Q}$ and of the rate of kinematic $\mathbf{q}$ generalised beam variables have been defined. The following generalised deformations are therefore introduced.

$$q_1=\frac{\mathrm{d}u_0}{\mathrm{d}x_1}+\frac{1}{2}\left(\frac{\mathrm{d}w_0}{\mathrm{d}x_1}\right)^2;\quad q_2=\frac{\mathrm{d}\theta}{\mathrm{d}x_1};\quad q_3=\theta+\frac{\mathrm{d}w_0}{\mathrm{d}x_1} \quad (30)$$

Indices 1, 2, 3 in the above equations denote the axial, bending and shear generalised components, respectively.

By assuming a linear elastic constitutive law for each layer, the generalised stresses and deformations can be connected through the following relations (31), (32).

$$\mathbf{Q}\equiv\begin{vmatrix}Q_1\\Q_2\\Q_3\end{vmatrix}=\begin{vmatrix}A_{11}&A_{12}&0\\A_{21}&A_{22}&0\\0&0&A_{33}\end{vmatrix}\begin{vmatrix}q_1\\q_2\\q_3\end{vmatrix}\equiv\mathbf{A}\mathbf{q} \quad (31)$$

$$A_{11}=\int_A E_1\,\mathrm{d}A;\quad A_{12}=A_{21}=\int_A E_1x_3\,\mathrm{d}A;\quad A_{22}=\int_A E_1x_3^2\,\mathrm{d}A;\quad A_{33}=\int_A G_{13}\,\mathrm{d}A \quad (32)$$

The elastic coefficients E_1 and G_{13} are the effective longitudinal and shear moduli obtained applying, on the initial configuration, the classical plate theory in the case of cylindrical bending.

By introducing eqns (29)–(31) in eqn (28), the following expression can be given to the contribution of the set of n layers to the internal power.

$$\sum_{i=1}^{n}\left(\int_{x_1}\mathbf{Q}^{\mathrm{T}}\dot{\mathbf{q}}^{*}\mathrm{d}x_1\right)_i=\sum_{i=1}^{n}\left(\int_{x_1}\mathbf{q}^{\mathrm{T}}\mathbf{A}\dot{\mathbf{q}}^{*}\mathrm{d}x_1\right)_i \quad (33)$$

3.2. Description of the interface

The description of the interface rests on its definition given in Section 2. With reference to Fig. 3, taken into account eqns (26), for the interface i ($i=1,\ldots,n-1$) the expressions of the displacement discontinuity in the global reference frame [eqn (1)] and of the mean displacement defining Γ [eqn (2)] result in:

$$\mathbf{u}_{\mathrm{m}}^{i}=\begin{vmatrix}u_{\mathrm{m}1}^{i}\\\mathbf{u}_{\mathrm{m}3}^{i}\end{vmatrix}=\frac{1}{2}\begin{vmatrix}u_{0\mathrm{m}}^{i}+x_3^{i+1}\theta_{\mathrm{m}}^{i}\\w_{0\mathrm{m}}^{i}\end{vmatrix};\quad [\mathbf{u}]^i=\begin{vmatrix}[u]_1^i\\[u]_3^i\end{vmatrix}=\begin{vmatrix}[u_0]^i+x_3^{i+1}[\theta]^i\\[w_0]^i\end{vmatrix} \quad (34a, b)$$

where, for a quantity y, the symbols y_{m}^{i} and $[y]^i$ have the following meaning

$$y_{\mathrm{m}}^{i}\equiv\frac{y^{i+1}+y^{i}}{2};\quad [y]^i\equiv y^{i+1}-y^{i} \quad (34c)$$

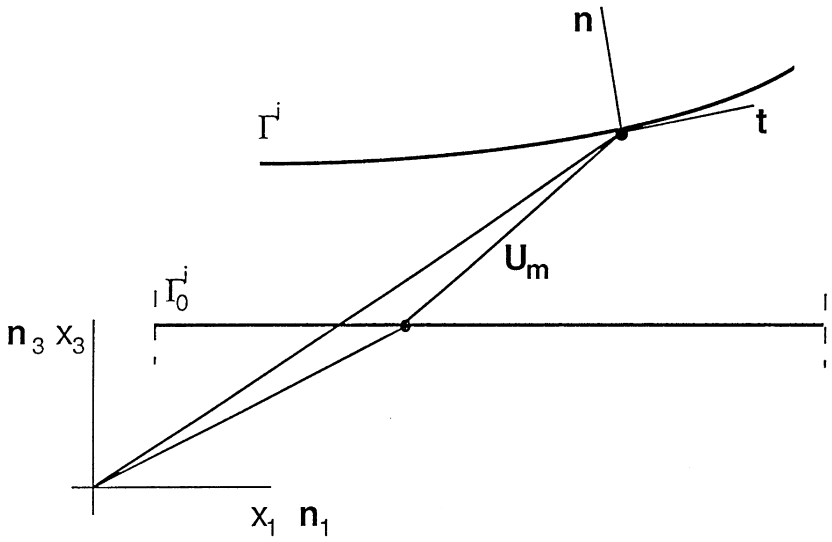

Fig. 5. Current configuration for an interface.

In order to be able to compute the internal power relevant to the interfaces, it is necessary to evaluate the components of the displacement discontinuity vector and of the velocity discontinuity vector in a local reference frame moving together with the interface. This is possible due to the definition of the interface [eqns (2) and (3)], which in the present case becomes (see Fig. 5):

$$\begin{vmatrix} x_{1\Gamma} \\ x_{3\Gamma} \end{vmatrix}^i = \begin{vmatrix} x_1 + u^i_{\mathrm{m}1} \\ x_c^{i+1} + u^i_{\mathrm{m}3} \end{vmatrix} \tag{35}$$

where $x_{1\Gamma}$, $x_{3\Gamma}$ are the coordinates of a point on Γ^i, in the current configuration. Equation (35) is a parametric representation of the interface, where the parameter is the coordinate x_1 in the initial configuration. It is, therefore, straightforward to derive the expression of the tangent **t** (not to be confused with the traction vector) and normal **n** vectors to the line and of the measure of the elementary length $\mathrm{d}\Gamma$ in the current configuration. With reference to the notation in Fig. 5, these are:

$$\mathbf{t} = \frac{1}{j}\left(\mathbf{n}_1\left(1+\frac{\partial u_{\mathrm{m}1}}{\partial x_1}\right)+\mathbf{n}_3\frac{\partial u_{\mathrm{m}3}}{\partial x_1}\right); \quad \mathbf{n} = \frac{1}{j}\left(-\mathbf{n}_1\frac{\partial u_{\mathrm{m}3}}{\partial x_1}+\mathbf{n}_3\left(1+\frac{\partial u_{\mathrm{m}1}}{\partial x_1}\right)\right) \tag{36}$$

$$\mathrm{d}\Gamma = \sqrt{\left(1+\frac{\partial u_{\mathrm{m}1}}{\partial x_1}\right)^2+\left(\frac{\partial u_{\mathrm{m}3}}{\partial x_1}\right)^2}\,\mathrm{d}x_1 \equiv j\,\mathrm{d}x_1 \tag{37}$$

In the above eqns (36), (37) $\mathbf{n}_1$ and $\mathbf{n}_3$ are the unit vectors directed as axes 1 and 3, respectively. The superscript i has been dropped for brevity, as done in the remaining part of this section. For numerical applications it is useful to express the velocity discontinuity vector in the local reference frame **n**, **t** as:

$$[\mathbf{v}] \equiv \begin{vmatrix} [v]_t \\ [v]_n \end{vmatrix} = \mathbf{R} \begin{vmatrix} [\dot{u}]_1 \\ [\dot{u}]_3 \end{vmatrix} = \mathbf{R}[\mathbf{v}]_{13}; \quad \mathbf{R} = \frac{1}{j} \begin{vmatrix} \left(1 + \dfrac{\partial u_{m1}}{\partial x_1}\right) & \dfrac{\partial u_{m3}}{\partial x_1} \\ -\dfrac{\partial u_{m3}}{\partial x_1} & \left(1 + \dfrac{\partial u_{m1}}{\partial x_1}\right) \end{vmatrix} \tag{38}$$

where $[\mathbf{v}]_{13}$ collects the components of the velocity discontinuity in the global frame 1–3.

The expression of the internal power relevant to the set of $n-1$ interfaces [eqn (9)] can therefore be re-written in a form useful for numerical computations (see Section 4):

$$\sum_{i=1}^{n-1} \left(\int_{\Gamma_i} \mathbf{t} \cdot [\mathbf{v}]^* \, d\Gamma \right)_i = \sum_{i=1}^{n-1} \left(\int_{x_1} \mathbf{t} \cdot \mathbf{R}[\mathbf{v}]^*_{13} j \, dx_1 \right)_i \tag{39}$$

In order to be consistent with the approximations introduced in Section 3.1 concerning eqns (28), the expressions of rotation matrix $\mathbf{R}$ and of the Jacobian j can be approximated as follows:

$$\tilde{\mathbf{j}} \cong \sqrt{1 + \left(\frac{\partial u_{m3}}{\partial x_1}\right)^2}; \quad \mathbf{R} \cong \frac{1}{\tilde{j}} \begin{vmatrix} 1 & \dfrac{\partial u_{m3}}{\partial x_1} \\ -\dfrac{\partial u_{m3}}{\partial x_1} & 1 \end{vmatrix} \tag{40}$$

3.3. Remarks

(i) The formulation adopted in Section 3.1 for a laminated beam could be extended to laminated plates. In the case of curved beams or shells, the formulation should suitably be completed with the equations representing a coordinate transformation from a reference, rectilinear, configuration to the real initial curved one.
(ii) The presented formulation is suitable for deriving finite elements for laminated beams and or plates.

4. Finite element model for rectilinear laminated beams and numerical solution strategy

The formulation presented in Section 2 and specialised in Section 3 to rectilinear laminated beams is here applied in a finite element context. Some detail on the spatial discretisation for the layers are given in Section 4.1, while in Section 4.2 the spatial discretisation for the interface is discussed. Due to the fact that geometrical and material instabilities are introduced in the formulation, the solution strategy deserve some discussion which is presented in Section 4.3.

4.1. Layer discretisation

To be consistent with the kinematic hypothesis of eqn of eqn (26), the generalised layer displacements $u_0^i(x_1)$, $w_0^i(x_1)$ and $\theta^i(x_1)$ are modelled by means of interpolation functions and nodal values, after a spatial discretisation along the direction x_1. For simplicity the discretisation must

be the same for all layers, in order to have corresponding nodes and nodal values. For each layer, implicitly assuming the assemblage of all finite elements along the layer, one can write:

$$\mathbf{s}^i(x_1) \equiv \begin{vmatrix} u_0^i(x_1) \\ w_0^i(x_1) \\ \theta^i(x_1) \end{vmatrix} = \mathbf{N}(x_1)\mathbf{U}^i \tag{41}$$

where $\mathbf{N}(x_1)$ is a matrix of shape functions and $\mathbf{U}^i$ collects the nodal parameters relevant to the layer i.

From the displacement model (41) (dropping the superscript i) the generalised layer deformations and deformation rate vectors [eqns (29), (30)] can be recovered after derivation; $\mathbf{q} = \mathbf{B}(\mathbf{U})\mathbf{U}$, $\dot{\mathbf{q}} = (\hat{\mathbf{B}}(\mathbf{U})\dot{\mathbf{U}}$. Due to the fact that with respect to a linear geometric case the only difference is in the expression of the first generalised deformation q_1, it is possible to give to matrices $\mathbf{B}(\mathbf{U})$ and $\hat{\mathbf{B}}(\mathbf{U})$ a particular form, which holds independently from the kind of finite element interpolations chosen.

$$\mathbf{q} = \mathbf{B}(\mathbf{U})\mathbf{U} \equiv [\mathbf{B}_{\mathrm{L}} + \mathbf{B}_{\mathrm{NL}}(\mathbf{U})]\mathbf{U}; \quad \dot{\mathbf{q}} = \hat{\mathbf{B}}(\mathbf{U})\dot{\mathbf{U}} \equiv [\mathbf{B}_{\mathrm{L}} + 2\mathbf{B}_{\mathrm{NL}}(\mathbf{U})]\dot{\mathbf{U}} \tag{42}$$

In the above equations, matrix $\mathbf{B}_{\mathrm{L}}$ is the finite element compatibility matrix which holds in the linear geometry case; matrix $\mathbf{B}_{\mathrm{NL}}(\mathbf{U})$ represents the modification of the first one due to the non-linear geometry effects.

After introduction of the interpolated fields in the expression of the internal power (33), its spatially discretised form can be obtained.

4.2. Interface discretisation

The spatial interpolation of interface quantities is here directly derived from that of the layers adjacent to the relevant interface. Starting from eqn (34b) and taking into account layer interpolation (41) for layers $i+1$ and i, the interpolated displacement discontinuity and velocity discontinuity vectors for the interface i can be given the following formal expression

$$[\mathbf{u}]^i(x_1) = \begin{vmatrix} [u]_1^i(x_1) \\ [u]_3^i(x_1) \end{vmatrix} = \mathbf{B}_{\mathrm{I}}(x_1)\mathbf{U}_{\mathrm{I}}^i; \quad [\mathbf{v}]^i(x_1) = \begin{vmatrix} [v]_1^i(x_1) \\ [v]_3^i(x_1) \end{vmatrix} = \mathbf{B}_{\mathrm{I}}(x_1)\dot{\mathbf{U}}_{\mathrm{I}}^i; \tag{43}$$

where the vector of nodal parameters $\mathbf{U}_{\mathrm{I}}^i$ involves nodal degrees of freedom pertaining to the layers adjacent to the interface and the assemblage of elements along the interface has been implicitly assumed as for eqn (41).

Interpolated fields (43) allow the discretisation of the internal power (39) relevant to the interface. Notice that the expressions (43) give the displacement discontinuity and velocity discontinuity vectors in the global reference frame. In order to practically use eqn (39), also the expressions of the rotation matrix $\mathbf{R}$ and of the Jacobian j must be found as functions of the nodal parameters governing the displacement fields. This can be done by means of expressions (38b) for $\mathbf{R}$, (37) for j and (34a) for the mean displacement $\mathbf{u}_{\mathrm{m}}^i$. $\mathbf{R}$ and j can, therefore, be considered known function of parameters $\mathbf{U}$.

4.3. Solution strategy

After spatial discretisation carried out as described in Sections 4.1 and 4.2, the problem introduced in Section 2, and specialised in Section 3, results to be governed by the discretised version of the principle of virtual powers and by an interface constitutive law of the kind described in Section 2.2.

4.3.1. Principle of virtual powers

Let U be the class of kinematically admissible nodal displacement rates and $\mathbf{P}$ the vector of equivalent nodal loads, the spatially discretised version of the pvp reads:

$$\int_{x_1} [\mathbf{U}^{\mathrm{T}}\mathbf{B}^{\mathrm{T}}(\mathbf{U})\mathbf{A}\hat{\mathbf{B}}(\mathbf{U}) + \mathbf{t}^{\mathrm{T}}(\mathbf{U})\mathbf{R}(\mathbf{U})\mathbf{B}_{\mathrm{I}} j(\mathbf{U})]\,\mathrm{d}x_1 \dot{\mathbf{U}}^* = \mathbf{P}^{\mathrm{T}}\dot{\mathbf{U}}^* \quad \text{for any } \dot{\mathbf{U}}^* \in \mathscr{V} \tag{44}$$

4.3.2. Interface constitutive law

For each interface i, the interface law imposed at a local level can be formally expressed as:

$$[\mathbf{u}]^i = \mathbf{R}\mathbf{B}_{\mathrm{I}}\mathbf{U}_{\mathrm{I}}^i; \quad \mathbf{t}^i = I([\mathbf{u}]^i, \chi^i) \tag{45}$$

In eqn (44) the contribution of each layer and interface have been formally assembled by implicitly defining matrices and vectors expanded at the global level of the laminate. For the sake of simplicity these are noted with the same symbols previously used for single layer and interface element contributions. The interface traction vector $\mathbf{t}$ depends on vector $\mathbf{U}$ (and on the past history in the case of irreversible interface models) through the interface law. In eqn (45) the interface constitutive law is only formally expressed as a relation between interface tractions $\mathbf{t}$ and interface displacement discontinuities $[\mathbf{u}]$; χ is a set of internal variables. The elastic constitutive law of the layers and the compatibility conditions are already introduced in eqn (44).

The response of the body is to be computed in a time interval $[0, T]$. By choosing convenient instants $0 = \tau_0, \tau_1, \ldots, \tau_{\mathrm{m}}$, the time interval is subdivided in time steps $\Delta\tau = \tau_{\mathrm{m}+1} - \tau_{\mathrm{m}}$. The response being known at a time instant τ_{m}, the global equilibrium equation (44), discretised in space through the finite element method, is solved at time instant $\tau_{\mathrm{m}+1}$. This is equivalent to solve the following non-linear system of equations in the unknowns $\mathbf{U}$:

$$\Phi(\mathbf{U}_{\mathrm{m}+1}) - \mu_{\mathrm{m}+1}\mathbf{P} = \mathbf{0} \tag{46a}$$

$$\Phi(\mathbf{U}_{\mathrm{m}+1} \equiv \int_{x_1} [\hat{\mathbf{B}}^{\mathrm{T}}(\mathbf{U}_{\mathrm{m}+1})\mathbf{A}\mathbf{B}(\mathbf{U}_{\mathrm{m}+1})]\,\mathrm{d}x_1 \mathbf{U}_{\mathrm{m}+1} + \int_{x_1} [\mathbf{B}_{\mathrm{I}}^{\mathrm{T}}\mathbf{R}^{\mathrm{T}}(\mathbf{U}_{\mathrm{m}+1})\mathbf{t}(\mathbf{U}_{\mathrm{m}+1})j(\mathbf{U}_{\mathrm{m}+1})]\,\mathrm{d}x_1 \tag{46b}$$

In the above equations, subscript $\mathrm{m}+1$ and m denote quantities computed at time instants $\tau_{\mathrm{m}+1}$ and τ_{m}, respectively; $\Phi(\mathbf{U}_{\mathrm{m}+1})$ represents the vector of internal forces; $\mu_{\mathrm{m}+1}$ is a load multiplier. Note that $\Phi(\mathbf{U}_{\mathrm{m}+1})$ can be considered as a known non-linear function of variables $\mathbf{U}_{\mathrm{m}+1}$. The dependence of $\mathbf{F}$ on $\mathbf{U}_{\mathrm{m}+1}$ is given by finite element interpolations and consequent definitions of $\hat{\mathbf{B}}(\mathbf{U}_{\mathrm{m}+1})$, $\mathbf{B}(\mathbf{U}_{\mathrm{m}+1})$, $\mathbf{R}(\mathbf{U}_{\mathrm{m}+1})$, $j(\mathbf{U}_{\mathrm{m}+1})$ and by the numerical integration on the time step of the interface law expressed in the term $\mathbf{t}(\mathbf{U}_{\mathrm{m}+1})$.

The solution of eqn (46) under load control can be carried out by directly applying an iterative

procedure, such as the Newton–Raphson method, in which the load factor μ_{m+1} is a known quantity and vector $\mathbf{U}_{m+1}$ the only unknown. With respect to a linear geometry case this obviously implies a more complex linearisation of function $\Phi(\mathbf{U}_{m+1})$.

In the presence of geometrical non-linearities and softening constitutive laws, of the kind introduced for the interface, the global behaviour can show snap-through or snap-back phenomena which cannot be treated by use of a load-controlled analysis. This is surely so in delamination tests where the response is generally unstable under load control and can also be unstable under displacement control (see Corigliano, 1993; Allix et al. 1994; Allix and Corigliano, 1996). For this reason an algorithm is used in which the controlled variable is neither the load factor nor the displacement in the charged point.

The algorithm in point can be considered of a Riks-type (Riks, 1972; Crisfield, 1981; Ramm, 1981) with a local constraint condition (Chen and Schreyer, 1990; Schellekens and de Borst, 1992; Daudeville and Ladavèze, 1993) and has been proposed in Corigliano (1993). The controlled quantity is a norm of the displacement jump increment vector, computed in the local reference frame associated to the current interface configuration, in the Gauss point S which result to be the most damaged one among those belonging to the set of points used for the evaluation of the interface law. Each step of the analysis consists of finding the solution of eqn (46) submitted to the following constraint condition:

$$\mathbf{c}^{\mathrm{T}}\Delta[\mathbf{u}]^{\mathrm{S}} - \beta = \mathbf{c}^{\mathrm{T}}\mathbf{B}^{*}(\mathbf{U}_{m+1} + \mathbf{U}_{m}) - \beta = 0 \tag{47}$$

In the above equation, $\mathbf{c}$ is a vector of weighting coefficients; β is a fixed parameter; $\mathbf{B}^{*}$ denotes the operator which connects, in an approximate form, the displacement discontinuity increment in point S in the local reference frame of the interface, to the global degrees of freedom vector:

$$\Delta[\mathbf{u}]^{\mathrm{S}} = (\mathbf{R}_{m+1}\mathbf{B}_{\mathrm{I}}\mathbf{U}_{m+1} - \mathbf{R}_{m}\mathbf{B}_{\mathrm{I}}\mathbf{U}_{m}) \cong \mathbf{R}_{m}\mathbf{B}_{\mathrm{I}}(\mathbf{U}_{m+1} - \mathbf{U}_{m}) \equiv \mathbf{B}^{*}\Delta\mathbf{U} \tag{48}$$

Vector $\mathbf{c}$ can be computed by making use of the results obtained at the end of the previous step:

$$\mathbf{c} = \frac{[\mathbf{u}]_{m}^{\mathrm{S}}}{\|[\mathbf{u}]_{m}^{\mathrm{S}}\|}; \quad \|[\mathbf{u}]\| = \sqrt{[u]_{n}^{2} + \|[u]_{t}\|^{2}} \tag{49}$$

Equations (46) and (47) result in a non-linear system in the unknowns $\mathbf{U}_{m+1}$ and μ_{m+1}; it is solved by an iterative procedure of the Newton–Raphson kind.

4.4. Remarks

(i) The interfacial connection is here seen as a surfacic medium, the stiffnesses of which are material properties. The 'ratio' of the interface and layer stiffness governs the decaying properties of the solution. The higher this ratio the more localised the solution is. The interlaminar stress distribution should always be correctly reproduced. Therefore, the mesh size should be chosen with respect to this ratio on the basis of the elastic solution. The initiation of the delamination process is greatly influenced by this ratio, while the subsequent propagation phase is much less influenced.

(ii) Interface discretisation and interpolations can in principle be chosen differently from those of adjacent parts as done in a different context in Bolzon and Corigliano (1997).

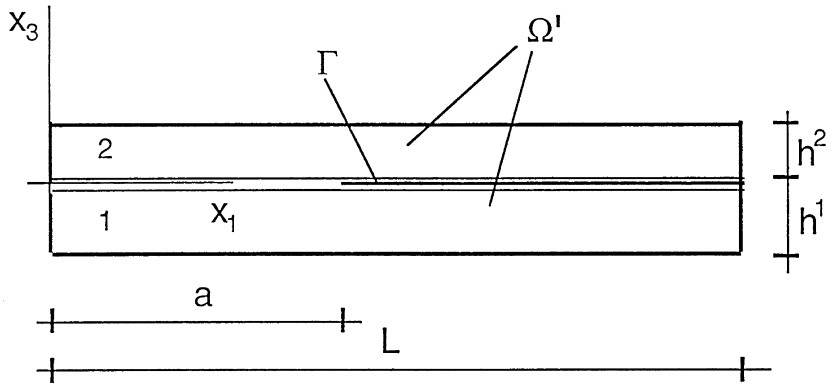

Fig. 6. Two superposed beams studied in the numerical examples.

(iii) In the nonlinear geometry case it is in general made use of an algorithm with a global constraint conditions such that the arc-length method. The comparison between the present local constraint approach and other used in the literature needs to be examined.

5. Numerical examples

In the present Section some numerical experiences concerning the simulation of laminated beams are presented. The formulation discussed in previous Sections is applied to the simple, but meaningful, case of a laminated beam composed of two layers only, which can partly be initially already disconnected, thus simulating an initial delamination. In these first examples the only significant material parameters is the critical energy release rate.

The definition of the geometrical parameters and the choice of the global reference frame are show in Fig. 6. The constant depth of the specimen is noted with B.

The chosen interpolation for layers 1 and 2 in Fig. 6 [eqn (41)] is based on finite elements which are linear for the displacement $u_0(x_1)$ and the rotation $\theta(x_1)$ (two interpolation parameters coinciding with the nodal values) and cubic of the Hermite type for the displacement $w_0(x_1)$ (four interpolation parameters coinciding with the nodal values and derivatives). Hence layer finite elements have eight nodal degrees of freedom.

In the chosen example the set Γ is reduced to a single interface identified by the coordinate $x_3^1 = 0$ in the initial configuration. The expression of interface quantities given in eqns (34) therefore simplifies as follows:

$$\mathbf{u}_{\mathrm{m}} = \begin{vmatrix} u_{\mathrm{m}1} \\ u_{\mathrm{m}3} \end{vmatrix} = \frac{1}{2} \begin{vmatrix} u_{0\mathrm{m}} \\ w_{0\mathrm{m}} \end{vmatrix}; \quad [\mathbf{u}] = \begin{vmatrix} [u]_1 \\ [u]_3 \end{vmatrix} = \begin{vmatrix} [u_0] \\ [w_0] \end{vmatrix} \tag{50}$$

As far as the interface discretisation is concerned, matrix $\mathbf{B}_{\mathrm{I}}$ in eqn (43), together with vector $\mathbf{U}_{\mathrm{I}}$ can be obtained after the use of eqns (50) and (41) specialised to the present case. As shown in eqn (50), the rotation θ does not appear in the expression of interface quantities due to the particular reference frame chosen; hence the nodal degrees of freedom involved in vector $\mathbf{U}_{\mathrm{I}}$ are

only those which govern the interpolations of functions $u_0(x_1)$ and $w_0(x_1)$ in the two adjacent layers, twelve totally. In order to complete the computations also the rotation matrix **R**, the Jacobian j and the contribution of the interface to the global tangent matrix must be derived.

In the following sub-sections 5.1–5.3 some meaningful examples which can be considered starting from the double-beam device of Fig. 6 are discussed.

The first example concerning a Double Cantilever Beam (DCB) test, is discussed in order to show that geometrical effects could in some cases be relevant in the analysis of classical interlaminar fracture tests. The second example shows the potentiality of the numerical model in following delamination induced by buckling. The third example is a classical one in the literature of buckling-induced delamination. Results similar to those obtained by e.g. Bruno and Grimaldi (1990) are here derived through the use of the numerical model based on interface laws presented in this paper.

5.1. Geometrical effects on a DCB specimen

As a first example it is here chosen to verify the influence of geometrical nonlinearities on the global response of a DCB specimen (Fig. 7).

The geometrical parameters, with the meaning of Fig. 6, are the following:

$$B = 1 \text{ mm}; \quad L = 20 \text{ mm}; \quad a_0 = 5.5 \text{ mm}; \quad h^1 = h^2 = 0.1\text{–}0.5 \text{ mm}$$

The above dimensions are all about one tenth of those used in practical experiences. The thickness of the layers varies in the range 0.1–0.5 mm in order to obtain different flexural stiffnesses and hence different degrees of influence of geometrical effects on the global reference.

The elastic parameters describing the layer behaviour are the Young modulus E_1 in direction 1 and the shear modulus G_{13} for shear in the plane 13.

$$E_1 = 135{,}000 \text{ MPa}; \quad G_{13} = 5700 \text{ MPa}$$

which are assumed to be the same for both layers.

In order to simulate the progressive delamination in pure mode I, an interface model of a bilinear

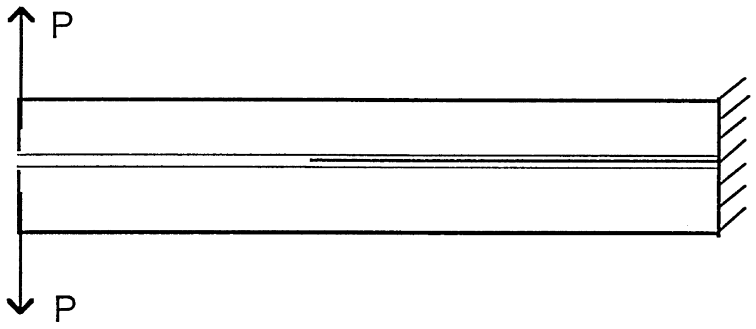

Fig. 7. Double Cantilever Beam test.

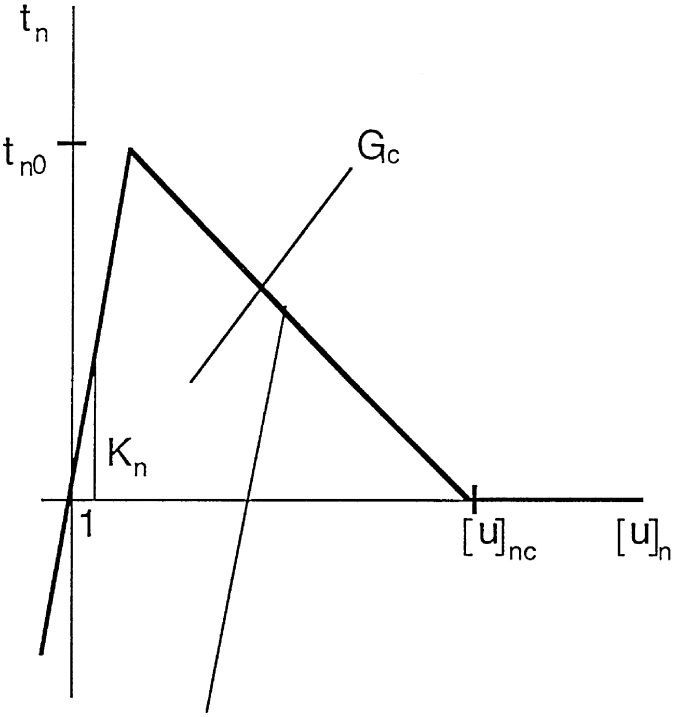

Fig. 8. Bilinear softening interface model.

softening kind such as that shown in Fig. 8, formulated in the framework of softening plasticity and proposed in a more general context in Corigliano (1993), has been used. The relevant material parameters, with the meaning of Fig. 8 are the following:

$$K_{\mathrm{n}}^{+} = K_{\mathrm{n}}^{-} = 1000{,}000\ \mathrm{N/mm^3}; \quad t_{\mathrm{n0}} = 50\ \mathrm{MPa}; \quad [u]\,0.016\ \mathrm{mm}; \quad G_{\mathrm{Ic}} = 0.4\ \mathrm{N/mm}$$

It is worth noting that in the present example, due to the symmetric loading of the DCB test, the interface Γ do not move from its initial configuration and remains always rectilinear.

The numerical simulations of the DCB test have been carried out under load control until an interface Gauss point results to be damaged for the first time, after this situation the analysis has been controlled locally, as described in Section 4.3.

The results of numerical analyses are shown in Fig. 9 in terms of load–displacement plots relevant to the loaded point at the extremum of one of the two arms of the specimen (Fig. 7). The different plots are obtained at varying thickness of both layers in the range above indicated. For each thickness the responses obtained with and without nonlinear geometry effects are compared in the figure. As expected, the influence of nonlinear geometry effects increases at decreasing thickness, i.e. at decreasing flexural stiffness of each layer.

A deeper discussion on nonlinear effects in the DCB delamination test and on other typical delamination tests is worthwhile and will be presented in a parallel work.

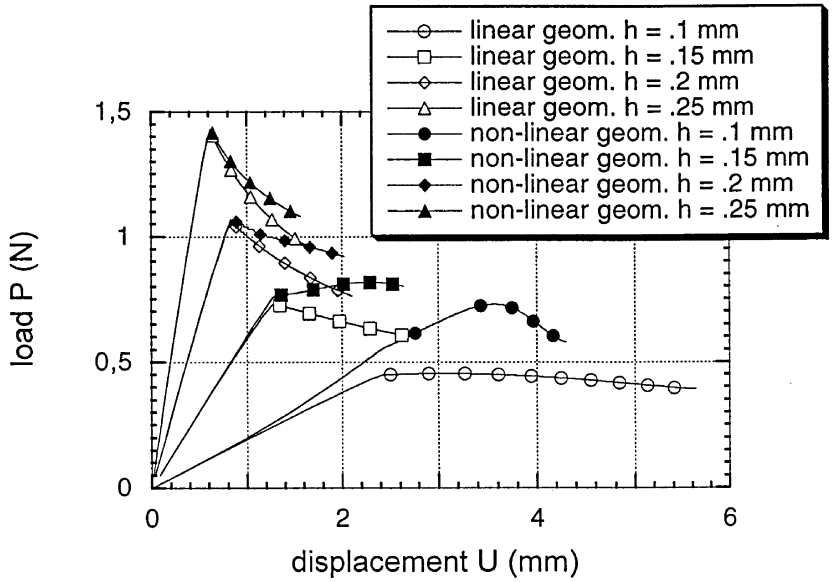

Fig. 9. Load–displacement plots for a DCB test at varying layer thickness.

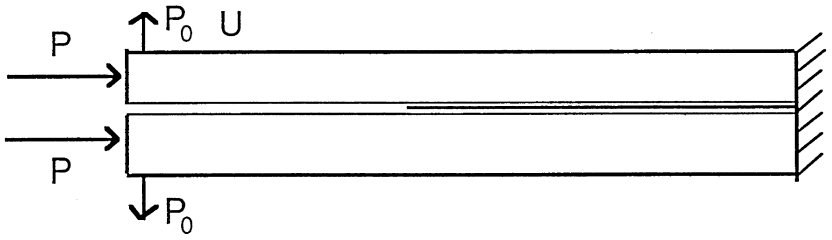

Fig. 10. Compressed cantilever beam with symmetrical perturbation.

5.2. *Buckling-induced delamination in a cantilever beam under compressive loading*

The second example discussed concerns a compressed beam, shown in Fig. 10. A fixed small perturbation loading $P_0 = 0.001$ N of a DCB kind is imposed on the two layers. The geometrical data are now the following:

$$B = 1 \text{ mm}; \quad L = 20 \text{ mm}; \quad a_0 = 5\text{–}10 \text{ mm}; \quad h^1 = h^2 = 0.2 \text{ mm}$$

The elastic parameters for the layers are the same as in sub-Section 5.1, while for the interface the same model of sub-Section 5.1 has been used at varying degrees of softening and Critical Fracture Energy G_{Ic}. The variation of G_{Ic} has been obtained at fixed value of limit stress t_{30} in the range $G_{Ic} = 0.02\text{–}1.6$ N/mm.

The numerical analyses presented have been carried out as in sub-Section 5.1, starting with a load control and then turning to a local control after an interface Gauss point has been damaged.

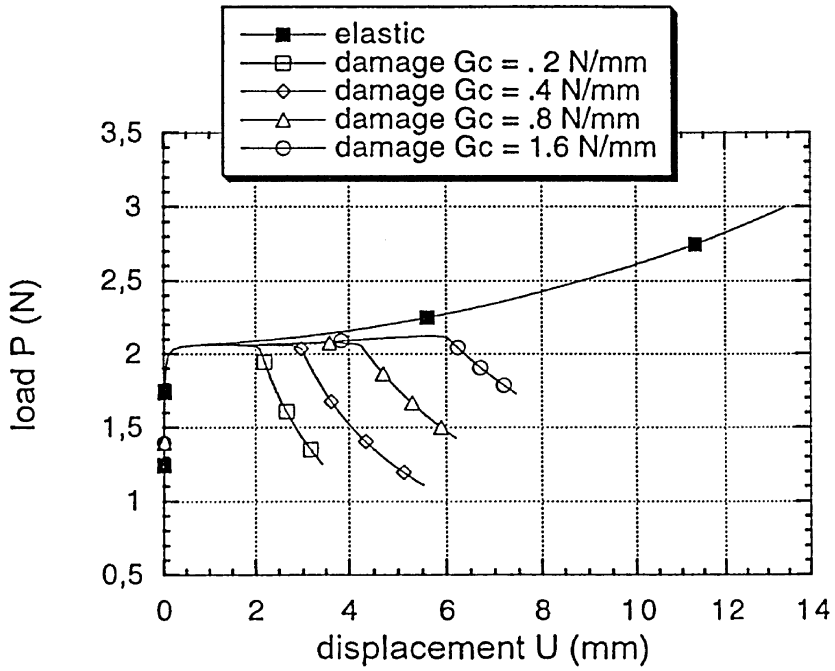

Fig. 11. Compressive load vs transversal displacement plots in a compressed cantilever beam with symmetrical perturbation at varying fracture energy.

In Fig. 11 plots of compressive load on a layer vs the vertical displacement of the layer end (Fig. 10) are shown. The behaviour of the beam with a non-damaging interface is that of an Euler cantilever beam with the length coinciding with that of the initial fracture a_0. At the critical load level the beam buckles and the deformed configuration is an amplification of the initial symmetric perturbation. The theoretical critical load value for a single layer given by the classical formula is:

$$P_{\mathrm{cr}} = \frac{\pi^2 EI}{4a^2} = 2.22 \text{ N}$$

where I is the inertia of a single layer. This value is almost reached by the numerical simulation. The difference should be attributed to the shear deformation not included in the classical formula.

After the buckling, the interlaminar tractions become important, this can lead to delamination as shown on Fig. 11 by the plots obtained with a damaging interface. In this case, in fact, the plot of load vs transversal displacement coincide with that of the elastic case until buckling; after buckling mode-I delamination starts and this is the reason of the softening part of the plot. From Fig. 11 it can also be seen that the starting point of delamination is postponed with increasing interface fracture energy G_{Ic}. In Fig. 12 the deformed configurations of the laminating beams at increasing time step are shown for the case with $G_{\mathrm{Ic}} = 0.4$ N/mm.

5.3. Buckling induced delamination in a built-in beam under compressive loading

The example here discussed consists in the simulation of the built-in beam with axial loading, symmetrical perturbation and central initial delamination of Fig. 13. The geometrical parameters

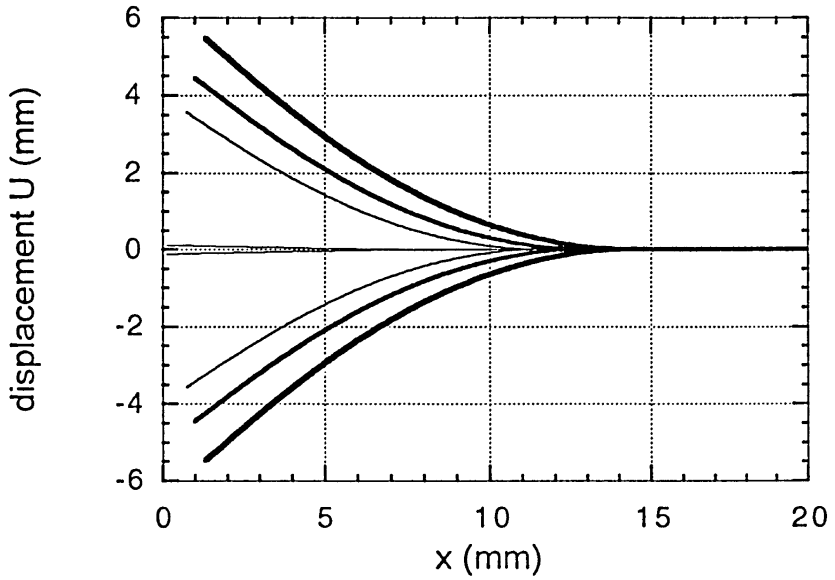

Fig. 12. Progressive delamination in a symmetrically perturbed compressed cantilever beam.

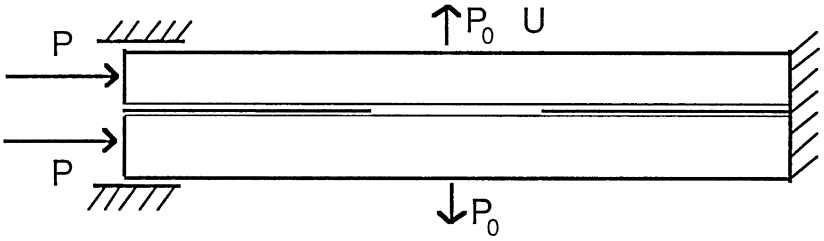

Fig. 13. Built-in beam with central delamination, under compressive loading and symmetrical perturbation.

are as in Section 5.2, with an initial length of the central delamination crack equal to 10 mm. The constitutive parameters for the layers are as in previous examples. The interface has been chosen to have the elastic–damage law of Section 2.2 with the following parameters:

$$K_n^+ = K_n^- = K_t = 100{,}000\ \text{N/mm}^3$$

$$a_n = a_t = 80\ \text{mm/N}; \quad \alpha = 1; \quad \gamma_n = \gamma_t = 0.121$$

which give a fracture energy $G_{Ic} = 0.4$ N/mm.

The elastic response of the specimen is now characterised by the competition between global and local buckling. The theoretical value of local buckling load is:

$$P_{\mathrm{cr}}^{\mathrm{loc}} = 4\frac{\pi^2 EI}{a^2} = 35.53 \text{ N}$$

where P is half of the global axial load (see Fig. 13). The theoretical value of global buckling load for a perfect beam (without central delamination a) coincides, in the present case, with $P_{\mathrm{cr}}^{\mathrm{loc}}$

$$P_{cr}^{\mathrm{glo}} = \frac{1}{2}\left(4\frac{\pi^2 E8I}{L^2}\right) = 35.53 \text{ N}$$

A theoretical evaluation of the global buckling load when a delamination crack is present is approximately given by the following formula:

$$wP_{\mathrm{cr}}^{\mathrm{glo}} \cong \left(\frac{L-a}{L}\right)\left(4\frac{\pi^2 E8I}{L^2}\right)+\left(2\frac{a}{L}\right)\left(4\frac{\pi^2 E2I}{L^2}\right) = 22.22 \text{ N}$$

where the inertia of the non delaminated ($8I$) and of the delaminated ($2I$) parts of the beam have been considered. An analysis with elastic interface has been first done with an non-symmetric perturbation $P_0 = 0.001$ N. The plot of axial load vs transversal displacement of one of the perturbed central point of the layers (Fig. 13) is presented in Fig. 14. The beam starts buckling, in

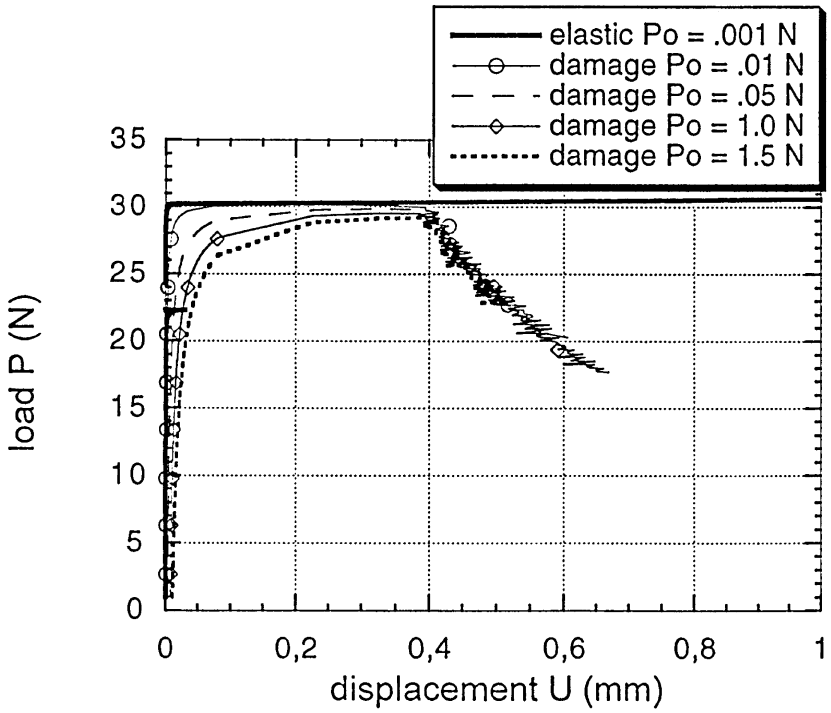

Fig. 14. Compressive load vs transversal displacement plots in a built-in beam under compressive loading and symmetrical perturbation.

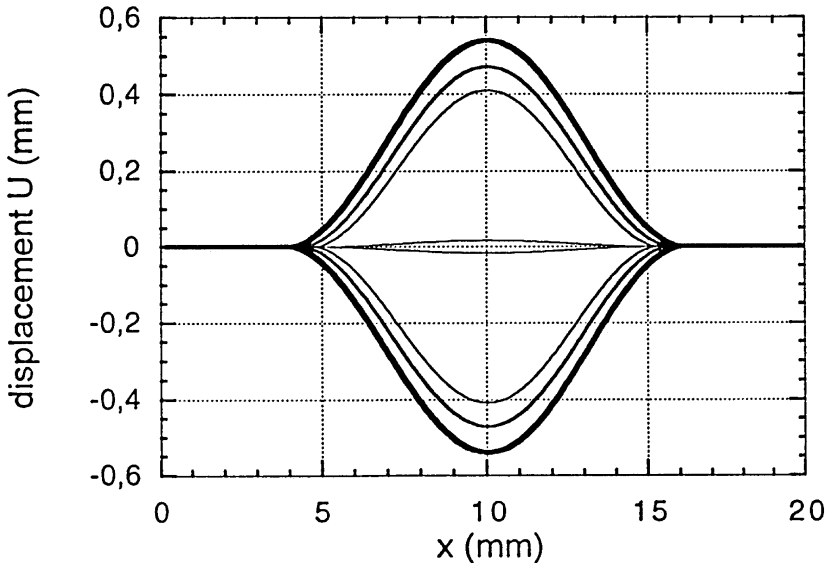

Fig. 15. Progressive delamination in a symmetrically perturbed compressed built-in beam.

a global mode, at a load of about 22.5 N which almost coincide with the above approximate evaluation. Subsequently the numerical response at increasing load looses the global buckling mode and reaches the level of about 31 N, at which local buckling is attained.

The elastic response is compared in Fig. 14 with those obtained with elastic–damage interfaces, at varying initial symmetric perturbation P_0 in the range $P_0 = 0.01$–0.15 N. In the damaging cases local buckling is attained, this is a cause of mode I delamination. The softening branches result to be almost independent from the initial perturbation. In Fig. 15 the deformed configuration for the symmetrical delamination is shown at different time steps.

6. Concluding remarks

In the present paper the problem of numerical simulation of delamination processes in the presence of important geometrical effects has been discussed. A unified formulation based on the use of interface models has been proposed. The treatment of geometrical nonlinearities and the parallel use of interface constitutive laws is allowed by the introduction of the fundamental hypothesis that displacement jumps along an interface are small. The proposed formulation has been specialised to rectilinear laminated beams and numerical aspects concerning the finite element implementation and the solution strategy have been discussed.

Some numerical examples concerning the propagation of delamination in interlaminar fracture specimens have been presented. In the examples the interaction between the interface degradation and the buckling of layers has been shown. More advanced numerical examples have to be treated

in order to fully demonstrate the interest of the proposed approach. In particular, examples concerning delaminations which initiate and then propagate, have to be solved.

The proposed interface modelling in a large displacement context allows in principle the simulation of the whole delamination process, from initiation to propagation and final failure. It can be coupled with plate and shell theories for laminated composites; it can and also be applied to other classes of problems such as that of the study of adhesives between rubber like materials.

Further studies should concern comparisons of the numerical procedure with experimental results; the introduction of true contact conditions in the laminated area.

References

Allix, O., Corigliano, A., 1996. Modeling and simulation of crack propagation in mixed-modes interlaminar fracture specimens. Int. J. Fracture 77, 111–140.

Allix, O., Ladevéze, P., 1992. Interlaminar interface modelling for the prediction of delamination. Composites Structures 22, 235–242.

Allix, O., Ladevéze, P., 1994. A meso-modelling approach for delamination prediction. In: Bazant, Z.P., Bittnar, Z., Jirasek, M. and Mazars. J. (Eds.), Fracture and Damage of Quasi-brittle Materials. E&FN Spon, London, pp. 606–615.

Allix, O., Ladevéze, P., Corigliano, A., 1994. Damage analysis of interlaminar fracture specimens. Composites Structures 31, 61–74.

Allix, O., Lévèque, D., Perret, L., 1996. Identification d'un modèle d'interface interlaminaire pour la prévision due délaminage dans les composites stratifiés. JNC10, AMAC Pub, pp. 1041–1052.

Bolzon, G., Corigliano, A. 1997. A discrete formulation for elastic solids with damaging interfaces. Comp. Meth. Appl. Mech. Engng. 140, 329–359.

Bottega, W.J., Maewal, A., 1983. Delamination buckling and growth in laminates. J. Appl. Mech. 50, 184–189.

Bruno, D., Grimaldi, A., 1990. Delamination failure of layered composite plates loaded in compression. Int. J. Solids Structures 26, 313–330.

Chai, H., Babcock, C.D., Knauss, W.G., 1981. One dimensional modelling of failure in laminated plates by delamination buckling. Int. J. Solids Structures 17, 1069–1083.

Chen, Z., Schreyer, H.L., 1990. A numerical solution scheme for softening problems involving total strain control. Computer Structures 37, 1043–1050.

Cochelin, B., Potier-Ferry, M., 1991. A numerical model for buckling and growth of delaminations in composites laminates. Comp. Meth. Appl. Mech. Engng 89, 361–380.

Cochelin, B., Daridon, L., Potier-Ferry, M., 1993. Delamination buckling and growth. In: Non classical problems of the theory and behaviour of structures exposed to complex environmental conditions, AMD, 164.

Corigliano, A., 1993. Formulation, identification and use of interface models in the numerical analysis of composite delamination. Int. J. Solids Structures 30, 2779–2811.

Crisfield, M.A., 1981. A fast incremental/iterative solution procedure that handles snap through. Computer Structures 13, 55–62.

Daudeville, L., Ladevèze, P., 1993. A damage mechanics tool for laminate delamination. Int J. Composite Structures 25, 547–555.

Evans, A.G., Hutchinson, J.W., 1984. On the mechanics of delamination and spalling in compressed films. Int. J. Solids Structures 20, 455–466.

Kachanov L.M., 1976. Separation failure of composite materials. Polymer. Mech. 5, 918–922.

Kanninen, M.F., 1973. An augmented double cantilever beam model for studying crack propagation and arrest. Int. J. Fracture 9(1), 83–92.

Kardomateas, G.A., 1993. The initial post-buckling and growth behavior of internal delaminations in composites plates. J. Appl. Mech. 60, 903–913.

Ladevéze, P., 1992. A damage computational method for composite structures. Computer Structures 44, 79–87.

Johnson, W.S. (Ed.), 1985. Delamination and debonding of materials. ASTM Special Technical Publication, 876, ASTM Philadelphia.

Pagano, N.J. (Ed.), 1989. Interlaminar response of composite materials. Composite Material Series 5, Elsevier, Amsterdam.

Ramm, E., 1981. Strategies for tracing nonlinear responses near limit points. In: Wunderlich, W., Stein, E., Bathe, K.J. (Eds.), Non-linear Finite Element Analysis in Structural Mechanics. Springer-Verlag, New York, pp. 68–89.

Riks, E., 1972. The application of Newton's method to the problem of elastic stability. J. Appl. Mech. 39, 1060–1066.

Schellekens, J.C., de Borst, R., 1992. Simulation of free edge delamination via finite element techniques. In: Ladevéze, P., Zienkiewicz, O.C. (Eds.), New advances in Computational Structural Mechanics. Elsevier, Amsterdam, pp. 397–410.

Storakers, B., Andersson, B., 1988. Nonlinear plate theory applied to delamination in composites. J. Mech. Phys. Solids 36, 689–718.

Storakers, B., Nilsson, K.F., 1993. Imperfection sensitivity at delamination buckling and growth. Int. J. Solids Structures 30 (8), 1057–1074.

Wang, S.S., 1983. Fracture Mechanics for delamination problems in composite laminates. J. Composites Mat. 17 (3), 210–213.

Whitney, J.M., 1989. Experimental characterization of delamination fracture In: Pagano, N.J. (Ed.), Interlaminar Response of Composite Materials. Composite Materials Series, 5. pp. 111–239.

Williams, J.G., 1988. On the calculation of energy release rates for cracked laminates. Int. J. Fracture 36, 101–119.